

Strain-dependent localization, microscopic deformations, and macroscopic normal tensions in model polymer networks

Carsten Svaneborg,^{1,2,*} Gary S. Grest,³ and Ralf Everaers²

¹*Max-Planck-Institut für Polymerforschung, Postfach 3148, D-55021 Mainz, Germany*

²*Max-Planck-Institut für Physik komplexer Systeme, Nöthnitzer Str. 38, Dresden, Germany*

³*Sandia National Laboratories, Albuquerque, NM 87185, USA*

We use molecular dynamics simulations to investigate the microscopic and macroscopic response of model polymer networks to uniaxial elongations. By studying networks with strands lengths ranging from $N_s = 20$ to 200 we cover the full crossover from cross-link to entanglement dominated behavior. Our results support a recent version of the tube model which accounts for the different strain dependence of chain localization due to chemical cross-links and entanglements.

PACS numbers: 83.10.Kn, 62.20.Dc, 61.41.+e

Cross-linking a melt of linear precursor chains leads to a polymer network which macroscopically behaves as a (viscoelastic) solid and which is microscopically characterized by a complex, quenched, random connectivity and topology [1]. Over the past sixty years a large variety of theories of rubber elasticity has been put forward [2, 3, 4], and there is a corresponding body of rheological literature devoted to comparing and testing the proposed stress-strain relations, see e.g. [5, 6]. Only recently, neutron scattering experiments [7, 8] and computer simulations [9, 10, 11, 12, 13] have begun to provide detailed microscopic information. Attempts to quantitatively correlate the microscopic and macroscopic response to strain were so far restricted to idealized model polymer networks with diamond lattice connectivity [11, 12].

In this Letter we report a comprehensive set of results from computer simulations of randomly end-linked model polymer networks [10, 13] under elongational strain. In our data analysis we follow the logic of most statistical mechanical theories of rubber elasticity [2, 3], i.e. we relate the localization of different parts of a polymer network to strain-induced microscopic deformations and the macroscopic elastic response [4, 14]. We focus on theories [1, 2, 15, 16, 17, 18, 19] based on Edwards' tube model [20], because the underlying ideas are conceptually relatively simple, (almost) completely worked out, and closely related to most modern theories of polymer rheology [14, 21]. Nevertheless, a key ingredient of the model, the strain and strand length dependence of the phenomenological tube diameter, remains controversial [22, 23]. Our data support a recent generalization of the tube model [15] which accounts for the different character of chain localization by cross-links [16, 17] and entanglements [2, 18, 19].

We used extensive Molecular Dynamics (MD) simulations to study the behavior of bead-spring polymer melts under uni-axial, volume-conserving elongation. The polymer model has two interactions that represent bonds and excluded volume, respectively. Interaction parameters are chosen to ensure conservation of the topological

state. The details of the simulation methodology can be found in the literature, see e.g. [10, 13]. The present Letter is based on simulations of end-linked networks of $M \times N_s = 5000 \times 20, 1000 \times 35, 2500 \times 100,$ and 3000×200 where M denotes the number of strands and N_s strand length. The state of the networks can be accurately characterized: the gel fraction is $> 99\%$, $> 91\%$ of the network is elastically active, and the fraction of four-functional crosslinkers is $> 78\%$, except for 62% in the case of the 3000×200 . Each network was simulated at several elongations ($\lambda_x = \lambda_{\parallel} = \lambda, \lambda_y = \lambda_z = \lambda_{\perp} = 1/\sqrt{\lambda}$). The networks were successively strained. After each strain increment the network was equilibrated, and configurations were sampled for more than 30 (2) Rouse times of the strands for the two short (long) strand networks, respectively. To reduce finite chain length effects the maximal elongations were limited to $\lambda = 2$ ($\lambda = 4$) for short (long) strand networks, respectively. Elastic properties were obtained by sampling the deviatoric part of the microscopic virial tensor defined as $\sigma_{\alpha\beta} = \langle \sum_{ij} F_{ij,\alpha} r_{ij,\beta} \rangle / V$, where the sum is over all pairs i, j of interacting beads, α, β are Cartesian indices, and F, r and V denote forces, separations and the volume, respectively. The normal tension is defined as $\sigma_T = \sigma_{xx} - (\sigma_{yy} + \sigma_{zz})/2$. In the following we present our simulation results together with a brief outline of the theoretical background.

With the tube model [20] Edwards proposed a tractable simplification of the complicated many-body problem of a randomly cross-linked and entangled polymer network. The key idea is that vulcanization leads to a permanent *localization* of the precursor chains (or, equivalently, long, randomly chosen paths through the network) in tube-like regions along the coarse-grained chain contours. In the following $d(\lambda_{\alpha})$ denotes the α 'th Cartesian component of the tube diameter, which depends only on the corresponding strain component λ_{α} , hence each elongation provides two tube diameters $d(\lambda_{\parallel})$ and $d(\lambda_{\perp})$. The zero-strain tube diameter $d(\lambda_{\alpha} = 1)$ is abbreviated d . The simplest measure of the tube diameter is the width, $d_X(\lambda_{\alpha})$, of the thermal fluctuations

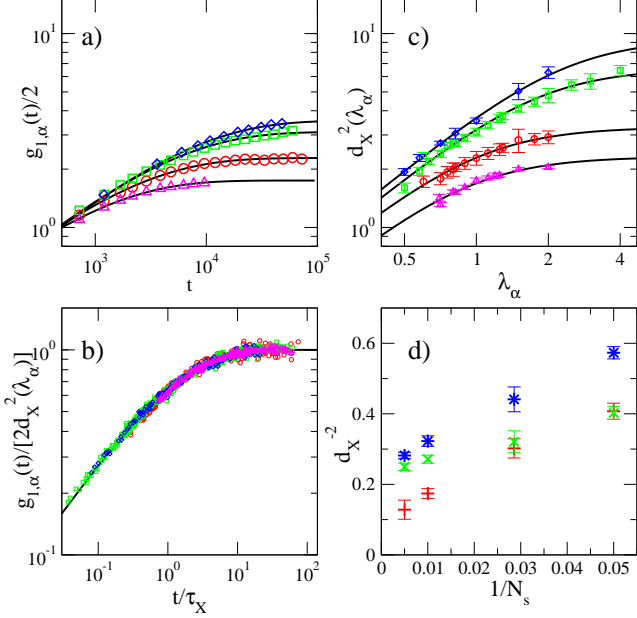


FIG. 1: (color online) Strain-dependent localization of crosslinks for $N_s = 20$ (magenta \triangle), $N_s = 35$ (red \circ), $N_s = 100$ (green \square), and $N_s = 200$ (blue \diamond). (a) Cross-link mean-square displacements as a function of time for the unstrained networks. Lines are fits of $2d_X^2(\lambda_\alpha)[1 - \exp(-\sqrt{t/\tau_X})]$ which we use to extract the tube diameters. (b) Rescaled cross-link mean-square displacements for all $\{N_s, \lambda_\alpha\}$ in comparison to the fit function. (c) Strain dependence of the tube diameter. The lines are fits of Eq. (1). (d) Strand length dependence of crosslinker confinement d_X (blue $*$), $d_{X,A}$ component (red $+$), and $d_{X,B}$ component (green \times).

of chemical cross-links around their average positions (Fig. 1). Our simulation runs are long enough to allow for a reliable extraction of d_X from the components of the mean-square displacements $g_{1,\alpha}(t) = \langle [r_\alpha(t) - r_\alpha(0)]^2 \rangle$, where the average is restricted to four-functional crosslinks (Figs. 1a and b).

The key issue is the non-trivial dependence of the extracted tube diameters on strain and strand length (Fig. 1c and d). From a theoretical point of view, the situation is relatively clear in the hypothetical case of “phantom networks” which consist of non-interacting Gaussian polymer chains [24]. The corresponding tube theory by Warner and Edwards (WE) [17] uses an isotropic, strain independent tube diameter $d_{X,A}(\lambda_\alpha) = d_{X,A}$, where $d_{X,A} \sim b\sqrt{N_s}$ is of the order of the root-mean-square extension of the network strands. The description of polymer networks as phantom networks becomes inappropriate, if the length of the network strands approaches the melt entanglement length, N_e [14, 21]. In particular, the tube diameter should become *independent* of strand length in the limit of very long strands where $d_{X,B} \sim b\sqrt{N_e}$. The strain dependence of entanglement dominated confinement is a subtle point. Empirical evi-

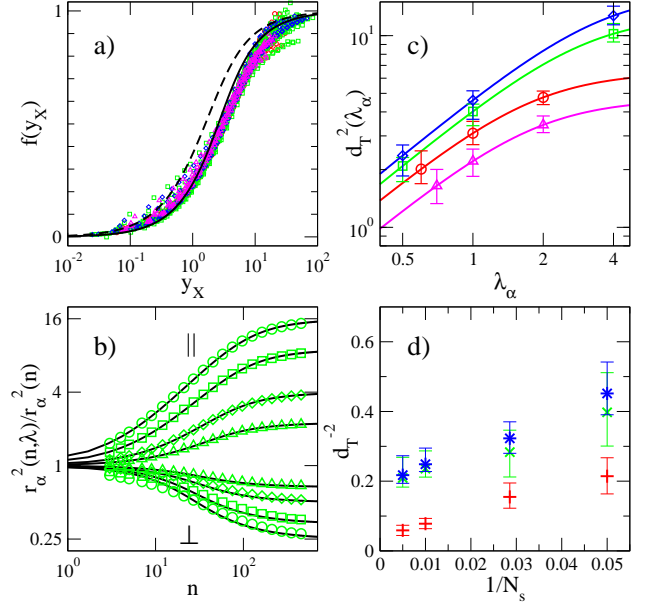


FIG. 2: (color online) Length scale dependent microscopic deformation response (symbols as in Fig. 1). (a) Scaling plot of the degree of affineness of the microscopic deformations using the tube diameters from Fig. 1c. The lines are f_A (dashed) and f_B (solid). (b) Parallel and perpendicular microscopic deformations for the 2500×100 system for strain $\lambda = 1.5, 2, 3, 4$ (symbols). Lines are fit of Eq. (3). (c) Strain dependence of the tube diameters. Symbols indicate the error bars and the range of λ_α covered by the data. (d) Strand length dependence of tube confinement d_T (blue $*$), $d_{T,A}$ component (red $+$), and $d_{T,B}$ component (green \times).

dence [8, 12] and theoretical arguments [2, 18, 19, 25] support the tube theories by Heinrich and Straube (HS) [2] and by Rubinstein and Panyukov (RP) [18] which predict an anisotropic, strain dependent tube diameter of $d_{X,B}(\lambda_\alpha) = \sqrt{\lambda_\alpha} d_{X,B}$.

Instead of combining an entanglement tube model with a classical theory of rubber elasticity in an ad-hoc fashion, the recently introduced double tube theory by Mergell and Everaers (ME) [15] accounts for the simultaneous presence of both effects with the help two correlated and additive confining potentials of the WE and the HS-RP type, respectively. The ME theory predicts

$$\frac{1}{d_T^4(\lambda_\alpha)} = \frac{1}{d_A^4} + \frac{1}{\lambda_\alpha^2 d_B^4}, \quad (1)$$

with an effective zero-strain tube diameter $d_T^{-4} = d_A^{-4} + d_B^{-4}$. As indicated by the solid lines in Fig. 1c, the individual data sets are well described by the functional form of Eq. (1). Moreover, the strand length dependence of the fitted cross-link and entanglement tube diameters $d_{X,A}$ and $d_{X,B}$ is in good agreement with the arguments underlying the double tube theory (Fig. 1d). It is worth noting the introduction of crosslinkers cause extra topo-

logical constraints, hence the observed narrowing of the entanglement tube for $N_s = 20$.

In the second part of our analysis, we consider microscopic deformations. In rubber-like materials, macroscopic deformations affect distances between neighboring monomers only weakly, while distances between distant monomers change affinely with the macroscopic strain. Following the logic of the tube model, we focus on the length scale dependent deformations of non-reversal random walk paths through the network. As a probe for microscopic deformations we utilize the mean-square distances $r_\alpha^2(n, \lambda_\alpha)$ between pairs of beads as a function of their chemical distance n . In a Gaussian theory $r_\alpha^2(n, \lambda_\alpha)$ fully specifies the microscopic conformations. In the absence of strain $r_\alpha^2(n) = b^2 n$, where b^2 is one Cartesian component of the mean-square segment length for a precursor chain. End-linking is known not to change the segment length compared to the precursor melt [10]. The crossover to affine deformations can be characterized by a dimensionless function [15]

$$f = \frac{r_\alpha^2(n, \lambda_\alpha) - r_\alpha^2(n)}{(\lambda_\alpha^2 - 1)r_\alpha^2(n)}, \quad (2)$$

with $0 < f < 1$. According to the tube model the crossover length should be of the order of d_X , i.e. f should be a function of $y_X = r_\alpha^2(n)/[2d_X^2]$. Fig. 2a verifies the interdependence of localization and microscopic deformations, which is an essential element of the tube model. Note that the plot contains *all* available data sets ($\{N_s, \lambda_\alpha\}$).

Theories based on the tube model make explicit predictions for the functional form of f (see the lines in Fig. 2a): $f_A(y) = 1 + (\exp(-y) - 1)/y$ [17] and $f_B(y) = 1 + 0.5 \exp(-y) + 1.5(\exp(-y) - 1)/y$ [15] were obtained in the limits of cross-link and entanglement dominated confinement, respectively. For the general case, the double tube model [15] predicts

$$f(y) = f_A(y) + \frac{d_{T,A}^4}{d_{T,B}^4 \lambda_\alpha^2 + d_{T,A}^4} [f_B(y) - f_A(y)], \quad (3)$$

where $y = r_\alpha^2(n)/[2d_T^2(\lambda_\alpha)]$ with $d_T(\lambda_\alpha)$ given by Eq. (1).

We determined $d_{T,A}$ and $d_{T,B}$ for each system by fitting Eq. (3) to the sampled $r_\alpha^2(n, \lambda_\alpha)$ for all values of λ_α simultaneously [30]. A typical result is shown in Fig. 2b. The effective strain-dependent tube diameters are shown in Fig. 2c, the two components $d_{T,A/B}(N_s)$ are plotted in Fig. 2d. As expected from the scaling plot Fig. 2a, there is qualitative agreement between the tube diameters d_X extracted from the cross-link fluctuations and d_T inferred from the analysis of the microscopic deformations. In particular, we observe a similar crossover to entanglement dominated confinement for long strands. Not surprisingly, there is no quantitative agreement between the two measures of the tube diameter. Tube models of rubber elasticity do not distinguish between middle monomers

of network strands (which are free to slide along the entanglement tube) and cross-linkers (which are not) [10]. In fact, the theories discussed in this Letter employ a simple harmonic localization potential which suppresses reptation-like motion.

In the third part of our analysis we consider the macroscopic elastic response of our networks. Fig. 3 shows the strain-dependence of the sampled normal tensions in the form of a standard Mooney-Rivlin plot [4]. This representation is commonly used to emphasize deviations from the classical stress-strain relation $\sigma_T(\lambda) \propto (\lambda^2 - \lambda^{-1})$. Similarly to experiments [4], we find that these deviations are more pronounced for entanglement dominated systems and that the shear modulus decreases with increasing strand length.

In polymer physics [4, 14] stresses are usually derived from chain conformations by dividing the chains into segments of length n . Segments are assumed to behave as independent entropic springs with spring constant $k_B T/r_\alpha^2(n)$. For a given monomer density ρ_m , the segment density is $\rho_s(n) = \rho_m/n$ [31]. Normal tensions derived from the virial tensor for this mesoscopic polymer model take a simple form involving only those ratios of mean-square internal distances which we have plotted in Fig. 3c:

$$\sigma_{T,Gauss}(\lambda) = k_B T \lim_{n \rightarrow 0} \rho_s(n) \left[\frac{r_\parallel^2(n, \lambda_\parallel)}{r_\alpha^2(n)} - \frac{r_\perp^2(n, \lambda_\perp)}{r_\alpha^2(n)} \right], \quad (4)$$

There are considerable subtleties in comparing the virial tensor calculated from the full microscopic interactions to the ‘‘Gaussian’’ normal tensions [28]. Fig. 3c shows that in the present case both quantities agree within the statistical error even though $\sigma_{T,Gauss}(\lambda)/\sigma_T(\lambda) \approx 90\%$. In contradiction to the arguments put forward in Ref. [9], we take the good agreement as quantitative evidence, that the tube representation of the network conformation in terms of *linear* paths through the network properly accounts for the relevant microscopic deformations.

The final step of our analysis is the *parameter-free* comparison in Fig. 3c of the measured stress-strain relations to the prediction of the ME theory [15]

$$\begin{aligned} \sigma_T(\lambda) &= (\lambda_\parallel^2 - 1)g(\lambda_\parallel) - (\lambda_\perp^2 - 1)g(\lambda_\perp) \quad (5) \\ g(\lambda_\alpha) &= \frac{\rho_m k_B T}{8} \frac{b^2}{d_T^2(\lambda_\alpha)} \frac{d_{T,A}^4 + 2\lambda_\alpha^2 d_{T,B}^4}{d_{T,A}^4 + \lambda_\alpha^2 d_{T,B}^4}, \end{aligned}$$

where we use the values of $d_{T,A}$ and $d_{T,B}$ from our fits of the microscopic deformations. The measured and the inferred normal tensions agree within the statistical error. To demonstrate the importance of the proper treatment of the deformation dependence of the confinement, we have also calculated stress-strain curves from the WE theory [17] ($d_T(\lambda_\alpha) = d_T \Leftrightarrow d_{T,B} = \infty$) and the HS-RP theory [2, 18] ($d_T(\lambda_\alpha) = \sqrt{\lambda_\alpha} d_T \Leftrightarrow d_{T,A} = \infty$). The comparison in Figs. 3a and b shows that attempts

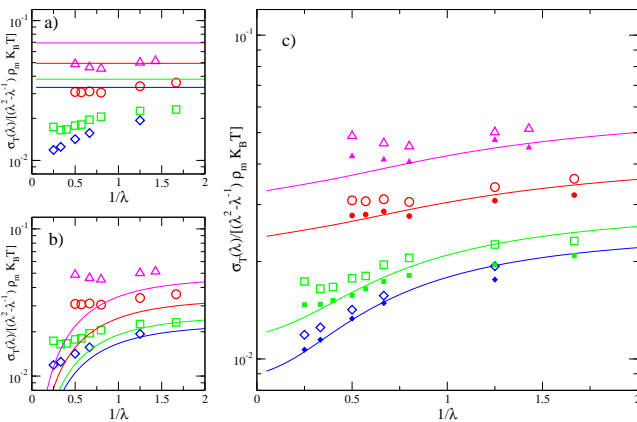


FIG. 3: (color online) Mooney-Rivlin plot of normal tensions as a function of strain: normal tensions sampled using the virial tensor (large symbols as in Fig. 1), and “Gaussian” normal tensions $\sigma_{T,Gauss}$ (small filled symbols) vs. theoretical predictions based on the analysis of the microscopic deformations (Fig. 2) (a) WE crosslinker tube theory, (b) HS-RP entanglement tube theory, (c) ME theory. Symbols and lines have a 10% and 30% error, respectively.

along these lines are restricted to estimates of the order of magnitude of the elastic response.

To summarize, we have used computer simulations to determine strain-dependent localization, length scale dependent microscopic deformations and macroscopic stresses in model polymer networks. Fig. 2a directly validates Edward’s original tube concept: on a scaling level the same length scale characterizes the spatial localization of chemical crosslinks and the crossover from local liquid-like to global solid-like behavior of the microscopic chain deformations. Closer inspection (Figs. 1/2 c,d) reveals the different character of (and the crossover between) cross-link and entanglement dominated confinement anticipated by the double tube model. In particular, Figs. 2 and 3 show that this model can *simultaneously* describe microscopic and macroscopic aspects of the response of our model networks to strain by accounting for the strain dependence of the (effective) tube diameter. While there clearly remain open questions concerning longitudinal fluctuations in the entanglement tube [3, 26, 27], we would like to emphasize that our simulations provide a substantially improved empirical basis for addressing these and similar problems in the controlled development of statistical mechanical theories of rubber elasticity. Currently, we are analysing the strain dependence of the primitive path mesh [29] in an attempt to systematically link the phenomenological tube model to the microscopic connectivity and topology of our model networks. Finally, we note that our simulations can also help to validate critical steps in the data analysis of (scattering) experiments addressing these issues.

We greatly acknowledge helpful discussions and a

long-standing collaboration with K. Kremer. We are particularly grateful to D. Heine for contributing data for 3000×200 networks. Sandia is a multiprogram laboratory operated by Sandia Corporation, a Lockheed Martin Company, for the United States department of Energy’s National Nuclear Security Administration under contract de-AC04-94AL85000.

* Electronic address: zqex@mpipks-dresden.mpg.de

- [1] R. T. Deam and S. F. Edwards, *Phil. Trans. R. Soc. Lond. A* **280**, 317 (1976).
- [2] G. Heinrich, E. Straube, and G. Helmis, *Adv. Polym. Sci.* **85**, 33 (1988).
- [3] S. F. Edwards and T. A. Vilgis, *Rep. Prog. Phys.* **51**, 243 (1988).
- [4] L. R. G. Treloar, *The Physics of Rubber Elasticity* (Clarendon, Oxford, 1975).
- [5] K. Urayama, T. Kawamura, and S. Kohijya, *Macromolecules* **34**, 8261 (2001).
- [6] M. Gottlieb and R. J. Gaylord, *Polymer* **24**, 1644 (1983).
- [7] S. Westermann, V. Urban, W. Pyckhout-Hintzen, D. Richter, and E. Straube, *Macromolecules* **29**, 6165 (1996).
- [8] E. Straube, V. Urban, W. Pyckhout-Hintzen, D. Richter, and C. J. Glinka, *Phys. Rev. Lett.* **74**, 4464 (1995).
- [9] J.-U. Sommer and S. Lay, *Macromolecules* **35**, 9832 (2002).
- [10] E. R. Duering, K. Kremer, and G. S. Grest, *J. Chem. Phys.* **101**, 8169 (1994).
- [11] R. Everaers and K. Kremer, *Macromolecules* **28**, 7291 (1995).
- [12] R. Everaers, *New J. Phys.* **1**, 12.1 (1999).
- [13] G. S. Grest, M. Pütz, R. Everaers, and K. Kremer, *J. Non-Crystal. Solids* **274**, 139 (2000).
- [14] M. Doi and S. F. Edwards, *The Theory of Polymer Dynamics* (Clarendon, Oxford, 1986).
- [15] B. Mergell and R. Everaers, *Macromolecules* **34**, 5675 (2001).
- [16] D. J. Read and T. C. B. McLeish, *Macromolecules* **30**, 6376 (1997).
- [17] M. Warner and S. F. Edwards, *J. Phys. A* **11**, 1649 (1978).
- [18] M. Rubinstein and S. Panyukov, *Macromolecules* **30**, 8036 (1997).
- [19] R. Everaers, *Eur. J. Phys. B* **4**, 341 (1998).
- [20] S. F. Edwards, *Proc. Phys. Soc.* **92**, 9 (1967).
- [21] T. C. B. McLeish, *Adv. in Phys.* **5**, 1379 1527 (2002).
- [22] D. J. Read and T. C. B. McLeish, *Phys. Rev. Lett.* **79**, 87 (1997); *Phys. Rev. Lett.* **80**, 5450 (1998).
- [23] S. Westermann, V. Urban, W. Pyckhout-Hintzen, D. Richter, and E. Straube, *Phys. Rev. Lett.* **80**, 5449 (1998).
- [24] H. James, *J. Chem. Phys.* **15**, 651 (1943).
- [25] G. Ronca and G. Allegra, *J. Chem. Phys.* **63**, 4990 (1975).
- [26] S. Edwards, H. Takano, and E. Terentjev, *J. Chem. Phys.* **113**, 5531 (2000).
- [27] M. Rubinstein and S. Panyukov, *Macromolecules* **35**, 6670 (2002).

- [28] J. Gao and J. H. Weiner, *J. Chem. Phys.* **103**, 1614 (1995).
- [29] R. Everaers, S. Sukumaran, G. Grest, C. Svaneborg, A. Sivasubramanian, and K. Kremer, *Science* **303**, 823 (2004).
- [30] All parallel and perpendicular components were fitted simultaneously, and logarithmically distributed chemical distances were used to avoid systematic errors due to a large number of strongly correlated points at large distances. The statistical error was estimated by a block analysis of the path ensemble. A systematic error was estimated by fitting the data restricted to $y \in [0.1 : 1]$ and $y \in [1 : 10]$ separately.
- [31] Treating the stress contributions of the elastically active and inactive parts of the network separately changes $\sigma_{T,Gauss}(\lambda)$ by less than 5%, as a consequence ρ_m has not corrected to account for this effect.